2019 2nd IEEE International Conference on Soft Robotics (RoboSoft)
COEX, Seoul, Korea, April 14-18, 2019

Toward a bio-inspired variable-stiffness morphing limb for amphibious robot locomotion

Robert L. Baines[1], Joran W. Booth[1], Frank E. Fish[2], and Rebecca Kramer-Bottiglio[1]

***Abstract*— Most robots operate either exclusively on land or in water. Toward building an amphibious legged robot, we present a morphing limb that can adapt its structure and stiffness for amphibious operation. We draw inspiration for the limb's design from the morphologies of sea turtle flippers and land-faring tortoise legs. Turtles and tortoises have rigid hulls that can be emulated in amphibious robots to provide a convenient, protected volume for motors, electronics, power supply, and payloads. Each of these animals' limbs are tailored for locomotion in their respective environments. A sea turtle flipper has a streamlined profile to reduce drag, making it apt for swimming. A land tortoise leg boasts a strong, expanded cross-section conducive to load-bearing. We capture the morphological advantages of both animals' limbs in our morphing limb via a variable stiffness composite coupled to a pneumatic actuator system that enables on-demand transitions between leg and flipper configurations. We control the degree of stiffness of the limb by varying electrical input to flexible heaters bound to the thermally responsive variable stiffness composite. The proposed morphing amphibious limb design is promising for enabling the next generation of hybrid soft-rigid robots to adapt to unstructured environments.**

I. INTRODUCTION

Amphibious robots represent a growing area of interest for roboticists. The ability to move both on land and in water with the same autonomous system has significant ramifications for security, industry, defense, and transportation. A looming challenge with amphibious robots is that in order to move through varying media, a robot must fundamentally adjust its means of locomotion. A classic solution, which has been explored extensively, is to rely on multiple distinct parts, such as wheels, rotors, and jets, to move on land or in water [1], [2], [3].

It is an attractive prospect to integrate multiple locomotion functionalities into one actuation space to prevent overburdening a robot's physical architecture. For example, serpentine robots can both swim and commute on land by varying their oscillation frequency and amplitude [4], [5]. In addition, fish [6] and salamander [7] locomotor strategies have inspired robots composed of connected modules which vary undulations to move both on land and in aquatic environments. Unfortunately, the many degrees of freedom of these robots creates a challenging control problem, diminishing their application scope. Moreover, oscillating serpent-inspired robot designs are not conducive to carrying larger payloads.

[1]Department of Mechanical Engineering & Materials Science, Yale University, 10 Hillhouse Avenue, New Haven, CT 06520, USA. (email: `rebecca.kramer at yale.edu`).

[2]Department of Biology, West Chester University, 730 S High St West Chester, PA 19383, USA.

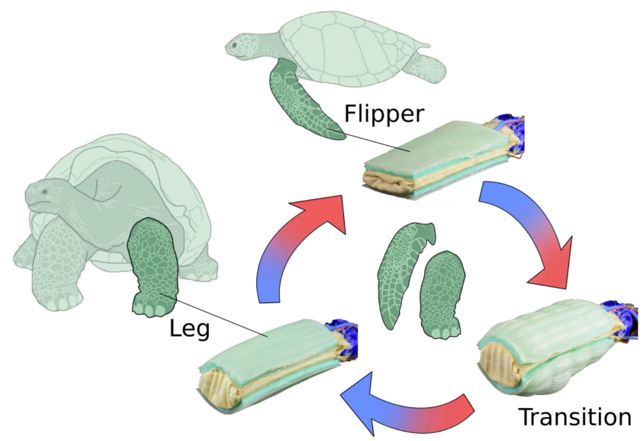

Fig. 1. We developed a morphing robotic limb intended for amphibious robots. Starting in a flipper state, the variable stiffness composite in the limb is subjected to heat via an embedded Joule-heated flexible heater, which softens it. Then, a pneumatic actuator pair is inflated to morph the limb to a transition state where it is held until the composite cools. At that point, pressure is no longer required to hold the leg configuration. Heating up the leg configuration again returns it to the flipper state.

A second approach to building amphibious robots strives to mechanically integrate swimming and walking mechanisms of legged robots, which have relatively simplified controller dynamics and have the capacity to transport payloads. One turtle-mimetic robot was designed with rigid legs equipped with passive hinged flaps that enabled both swimming and walking [8]. On the upstroke during swimming, the hinged flaps allowed the leg to move through water without much resistance. On the power stroke, the flap snapped into place against the leg, providing a large surface area for propulsive force. Another robot was shown to transform its hybrid wheel-leg system to accommodate different terrains [9]. Yet another robot morphed its legs from a walking to a swimming configuration using clutch-activated interlocking rigid segments [10].

The aforementioned approaches to integrate walking and swimming functionality pose elegant solutions, but they exhibit a lack of environmental versatility because they rely on rigid components. A wealth of useful environmental adaptations are untenable since their mechanisms have a fixed stiffness associated with each limb state. For instance, if a robot is swimming in water with obstacles, it is preferable to decrease its limb stiffness so that the system can sustain impacts without breaking. In nature, such structural compliance protects the appendages of a number of biological

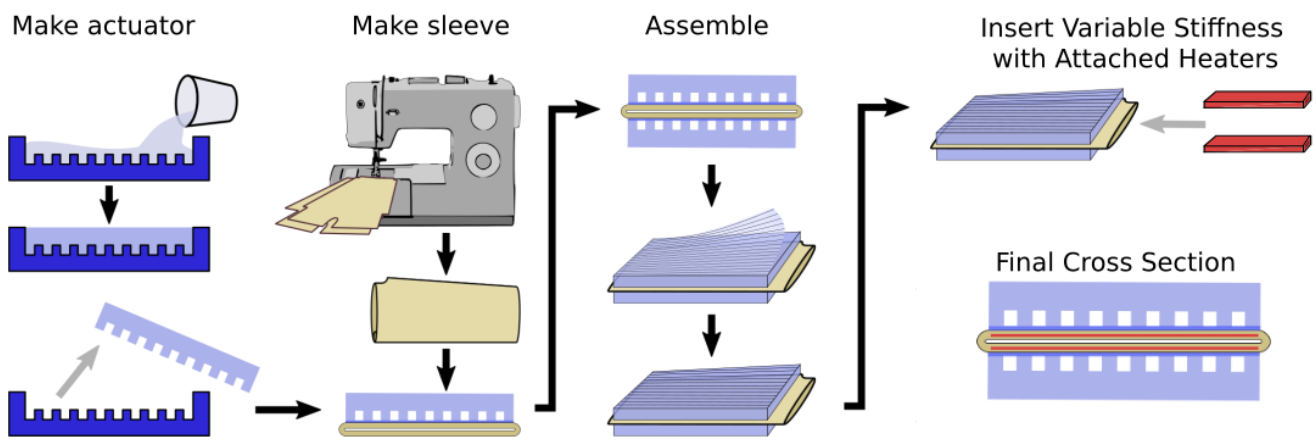

Fig. 2. Manufacturing the morphing limb can be separated into four distinct steps. First the actuators were cast from elastomer in an acrylic mold. Then they were attached to a fabric sleeve. Next, unidirectional fabric was bonded to the top of the actuators. Lastly, the variable stiffness composite-foil heater system was inserted into designated pockets in the fabric sleeve.

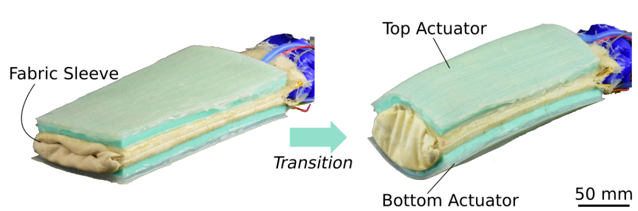

Fig. 3. The morphing limb is approximately 170 mm long, 85 mm wide at the bottom, tapered to 75 mm wide at the top, 30 mm thick in the flipper stage, and expands to a ~70 mm diameter in the leg stage.

organisms, notably winged insects, from shattering when they are subjected to large impacts [11]. Similarly, if the robot is transitioning from water to land, an intermediate limb stiffness has been shown to be optimal for moving efficiently [12]. It is therefore useful to be able to tune the stiffness of a locomotion mechanism on an amphibious robot. Recent work has demonstrated how variable stiffness limbs can allow an amphibious robot to move effectively through various environments [12]. The author's presented approach utilizes a mechanism with five stiffness presets. Changes in stiffness are accomplished by adjusting the height of the limbs relative to their connection on the robot. This coupling between geometry and stiffness constrains a robot's adaptive abilities. For instance, the robot cannot use the length of its fully extended leg at a high stiffness. It is desirable to have independent control over geometry and stiffness in an amphibious robotic limb. Further, the only way to change between stiffness presets on the robot is to do so manually, prior to deploying the robot. As a result, the stiffness of its leg cannot change *in-situ*. To fully realize the advantage of autonomous legged amphibious robots, limb stiffness change must be able to occur without manual intervention.

We approach the challenge of developing amphibious robots by observing the limb shapes of two morphologically similar animals: sea turtles and tortoises. Sea turtles have flippers with profiles apt for efficient lift-based swimming [13]. Thin and cambered, sea turtle flippers can cut through water with minimal drag [14]. On the other hand, tortoises have highly stable cylindrical cross-section legs that allow them to bear and walk under the often substantial weight of their carapaces. Herein, we create a limb which can transform from the shape of a sea turtle flipper to a tortoise leg (Figure 1). We accomplish this through use of a variable stiffness material-pneumatic actuator system. In particular, the limb can morph from a flipper to a leg phase when the variable stiffness materials inside are softened via Joule-heated flexible copper heaters, and the antagonistic pneumatic actuator pair on the exterior is inflated, deforming the materials. The limb can sturdily retain a leg shape after the variable stiffness material cools below its glass transition temperature (T_g) of 30-40°C and hardens. Holding the air pressure inside the actuators is thus no longer needed. Morphing back to the flipper phase is achieved by re-heating the variable stiffness elements past T_g, which relaxes them back to the initial, flat geometry in which they were cast. This described sequence of operation for the morphing limb prototype is pictured in Figure 1.

With this work, we unlock an unprecedented spectrum of limb stiffnesses and topologies which we can use to optimize amphibious robot locomotion within a particular environment: water, land, or littoral zones. An additional benefit of our approach is robustness, specifically when compared to previously reported amphibious robotic limbs composed of rigid metal components. The inherently corrosion-resistant and vibration-immune materials in our system make it highly viable for unstructured, dynamically changing amphibious environments.

II. Fabrication of Components of the Morphing Limb

The morphing limb comprises three major subsystems. The first subsystem is composed of two actuators that induce the bending deformation of the limb, allowing it to transition from a flipper to a leg state. The second subsystem constitutes the variable stiffness layers and paired heaters that are used to soften the variable stiffness material on demand. The third subsystem is the fabric sleeve that holds the actuators and variable stiffness layers together. Figure 2 details how all of these subsystems are integrated together in the manufacturing process of the morphing limb, and Figure 3 shows the final prototype in its two configurations. In subsequent sections, we elaborate on each component used in the manufacturing process.

1) Actuator: There are two identical actuators on the morphing limb. Each actuator is an extension of the traditional Pneunet actuator [15], but with added unidirectional fabric on its top to further direct inflation deformation along the longitudinal axis of the limb. More recent updates to the Pneunet actuator, such as fiber wrapped actuators [16], could not be applied because it is impractical to wrap tension limiters around the length of a large, planar area.

The actuators were cast in laser-cut acrylic molds from a platinum-cure silicone rubber with Shore hardness 10 (Dragon Skin 10A, Smooth-On). The mold was degassed in a vacuum chamber after which a flat lid and heavy weight was placed on top of the mold to improve flatness and dimensional accuracy between batches. Then, the actuators were attached to a fabric sleeve, which acted as the primary strain limiting layer to induce bending. Next, a unidirectional fabric was bonded to the top of the actuators such that the fibers were aligned along the length of the limb. The addition of this fabric helped direct actuator deformation. Lastly, the variable stiffness composite and heater system was inserted, completing the assembly.

2) Variable Stiffness Composite and Resistive Heater: The variable stiffness composite is composed of a two-part epoxy system mixed with graphite particles, imbued in a plain-weave cotton fabric. The epoxy is a thermoset that decreases by two orders of magnitude in bending stiffness past a T_g of 30-40°C [17]. This quality allows the material to be deformed into different geometries when it is softened. Upon cooling, it retains the newly deformed shape. When heated yet again, stress relaxation in the material forces it back to its initial configuration with some hysteresis. We utilize this mechanism to morph back and forth between the flipper and leg states.

The variable stiffness layer was created by mixing 28% wt. Jeffamine D400 (Hunstaman International, LLC), 69% wt. EPON 828 (Momentive Performance Materials Inc.) and 3% wt. expanded graphite. The thermoset epoxy enables variable stiffness; the low percentage conductive carbon filler enhances stiffness and thermal conductivity. The carbon filler was created by expanding sulfuric-acid intercalated graphite (Sigma-Aldrich) at 800°C, adding the expanded graphite to cyclohexane to create a 1% wt. graphite mixture, and subjecting it to sonication for 4 hr (QSonica Q700 Ultrasoniator). The resulting graphite nanoparticles have approximately 50 nm diameter. Lastly, the mixture was dried and blended into a fine powder to elicit the final graphite particulates. The epoxy and graphite particulates were mixed vigorously and imbued into a muslin fabric sheet by rod coating. The fabric serves as reinforcement to enhance the strength of the composite material, reduce its brittleness, and provide a host structure for achieving a thin composite. The uncured composite was then placed in an incubator for 12 hr at 70°C, with a heavy flat plate on top to disperse the resin homogeneously through the fabric during cure.

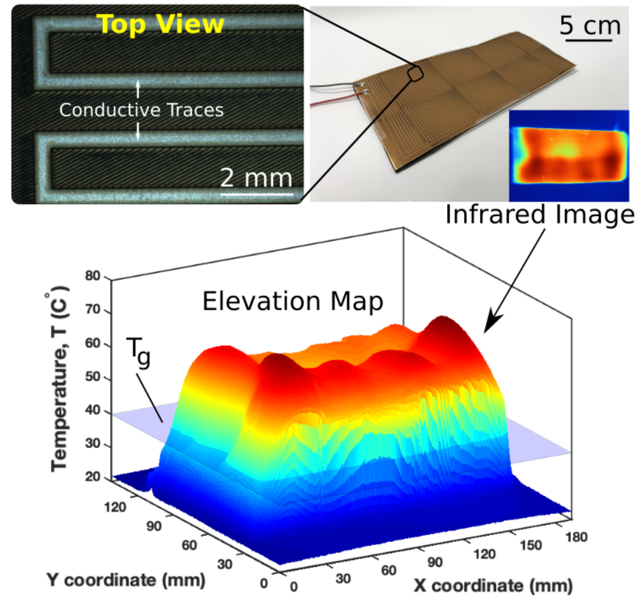

Fig. 4. Flexible heaters were fabricated by laser etching thin kapton-clad copper foil to produce a serpentine conductive trace pattern, as shown in the microscope top view inset. We adhered these heaters to the variable stiffness composite for on-demand limb stiffness changes. We validated that the heater could effectively and uniformly heat the material through thermal imaging. Here, the heater was subjected to 72 W for one min in free-convection conditions. The infrared image (top-down view) was translated to a elevation map (3D) that indicates nearly all of the composite system is above the max end of the glass transition temperature, save extreme peripheral regions.

A resistive heater was coupled to the variable stiffness composite to change its stiffness on-demand. The resistive heater is thin and flexible. As a result, it is easily integrated with the variable stiffness layer. The resistive heater was created by surface etching 0.127 mm thick copper-clad kapton (DigiKey) in a ProtoLaser U4 (LPKF laser and electronics). A serpentine patterned trace 0.70 mm wide, covering an area of 4110.05 mm^2 was found to produce uniformly heat-dissipating specimens with a resistance of 12 Ω. A thin layer of thermal grease (Chemplex 1381 DE, FUCHS) was dispersed between the variable stiffness composite and the heater to facilitate heat transfer. We validated that the heater was able to heat above T_g and homogeneously heat the material it was attached to. Figure 4 showcases the thermal map of the heater system in free-convection, after having been subjected to 72 W for one min. This composite-resistive heater stack-up was then placed inside a pocket in the fabric sleeve detailed in the next section.

3) Fabric Sleeve: The fabric sleeve was designed to hold the variable stiffness layers and actuators together and provide a hinge along each edge of the actuators. The fabric sleeve consists of two layers of fabric with seams that create two pockets, as well as a cavity that allows the limb to expand without resistance when it is transforming to the leg phase. Variable stiffness layers reside in the larger two pockets. The actuators were bonded to the exterior of the sleeve.

III. Test Procedures and Results

1) Compression analysis of morphing limb: To characterize the load-deformation relationship of the flipper and leg phases of the morphing limb, we conducted quasi-static compression tests with an Instron 3345 fitted with a 5 kN load cell. Additionally, we varied the temperature input to the material system in the flipper configuration to highlight the effects of geometric stiffness versus material stiffness.

Custom-fabricated parallel plates served to constrain the flipper from sliding as it was being compressed. The plates contained a notch where the top and bottom of the flipper fit snugly. Five trials at three distinct temperatures, 21°C (room temperature), 30°C, and 40°C, were conducted for the flipper, for a total of 15 independent tests. We specifically chose a swath of temperatures so as to include the top and bottom temperatures in the glass transition range of the variable stiffness composite (30°C to 40°C). We pre-cycled the flipper with embedded variable stiffness composite heated to 40°C 10 times before running tests to remove early cycle hysteresis effects. A test of five trials of the flipper without any variable stiffness material inserts was conducted to serve as a baseline comparison. With the limb placed between the custom-made parallel plates, we compressed it at 40 mm/min, stopping when the force dropped beyond a 2% threshold or more (*i.e.* when the flipper buckled), or when it reached 50 mm displacement.

In addition to the flipper phase, five compress-to-failure trials at room temperature were performed on the leg configuration with different variable stiffness materials each time. We did not subject the leg phase to different temperatures because the leg geometry is intended for load-bearing on solid land. Additionally, the mechanism by which the leg phase morphs back to the flipper phase is stress relaxation induced by heating (*i.e.* a warm leg configuration cannot be sustained, since no input pressure would hold it in place). Note that in tests for both the leg and flipper conditions, we did not inflate the pneumatic actuators; presented is only the stiffness of a final transformed geometry.

Figure 5A shows the results of the compression tests conducted on the flipper phase of the morphing limb. The darker colored trend line indicates the mean, and the lighter color clouds indicate one standard deviation from the mean. Evidently, the flipper without any material insert (black) exhibits lowest stiffness and does not buckle before 50 mm. The flipper with variable stiffness material inserts heated uniformly to the top end of T_g (red) is slightly stiffer and does not buckle either. The flipper achieves an intermediate

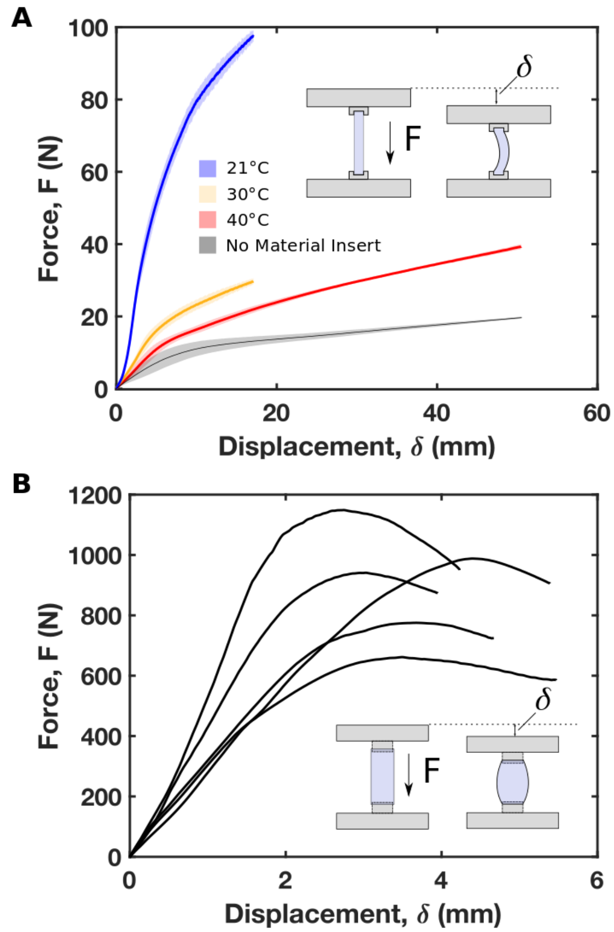

Fig. 5. A) Compression test results for the flipper state of the morphing limb at various temperatures, as well as the system without the variable stiffness material as a comparison baseline. The higher the induced temperature, the softer the system becomes. In the absence of a variable stiffness material, the limb is the softest. B) Compression test results for the leg state of the morphing limb at a single temperature (21°C). Note the leg is much stiffer than the flipper. This result is a direct consequence of the geometric stiffness provided by the cylindrical geometry of the leg.

stiffness when heated at the beginning of T_g (orange), and buckles around 18 mm. Finally, the flipper is stiffest when the variable stiffness inserts are at room temperature (blue). The maximum force it sees before buckling is 98 N. Note that the trends that buckled (orange and blue) were truncated to extend only as far as the specimen out of five that buckled the earliest.

Figure 5B showcases the compress-to-failure test results for the leg phase at room temperature (21°C). Five individual specimens are reported as their own lines to visualize the extent of variation between samples, which was greater than that witnessed for the flipper compression tests. A primary reason for this variation likely stems from manufacturing processes; that non-uniformities in the fiber-epoxy composite elicit pronounced stress concentrations when the limb is subjected to loading. This hypothesis is partly verified by the different modes of buckling and cracking observed when extracting the variable stiffness material specimen from the limb after each test. Another reason for the variation is likely nuances in limb alignment–which are exaggerated by the high force scales–when placed in between the plates.

The maximum compression force seen by the leg without buckling was approximately an order of magnitude higher than the flipper at room temperature: 1100 N. Further, the leg phases buckled under less displacement on average–around three to five mm compared to the flipper. These two facts underscore the significant role geometric stiffness plays in the limb's load-bearing capabilities. In fact, it is known that hollow cylinders are an optimal load-bearing geometry for columns under compression, which verifies this experimental observation.

Further insight into the buckling behavior of the two limb states under compression at room temperature can be attained by treating them as columns under compression. Modeling the leg as a cylindrical cross-section column and the flipper as a rectangular cross-section column, we have the following area moments of inertia:

$$I_{leg} = \frac{\pi}{4} r^4 \tag{1}$$

$$I_{flipper} = \frac{bh^3}{12} \tag{2}$$

Where r is the radius of the leg cross section, b is the width and h is the height of the flipper cross section. The Euler critical or maximum load which a limb can bear without buckling is defined as:

$$P_{cr} = \frac{\pi^2 EI}{(kL)^2} \tag{3}$$

Where E is the modulus of elasticity of the material (the same for leg and flipper configurations), I is the area moment of inertia of the limb cross section, k is the effective length factor given as 1 for two pin boundary conditions (we assume pinned because the limb is free to rotate about the contact point of its plate constraints), and L is the unsupported length of the limb (again, which is the same between each configuration). The ratio of the critical load for the leg to the flipper gives insight into how much more load the leg can sustain without buckling, and given the previous conditions, simplifies to:

$$\frac{P_{cr,leg}}{P_{cr,flipper}} = \frac{I_{leg}}{I_{flipper}} = \frac{\frac{\pi}{4} r^4}{\frac{bh^3}{12}} \tag{4}$$

With $r = 32$ mm, $b = 80$ mm, and $h = 23$ mm, we see that for the case of our morphing limb:

$$\frac{P_{cr,leg}}{P_{cr,flipper}} = 10.15 \tag{5}$$

This is approximately the ratio of buckling force exhibited by the leg (max around 1100 N) to the flipper (max around 100 N) in Figure 5A and B, and validates experimental results. It is straightforward to tune the thicknesses of the morphing limb system to achieve a desired force at which each configuration, leg and flipper, buckles.

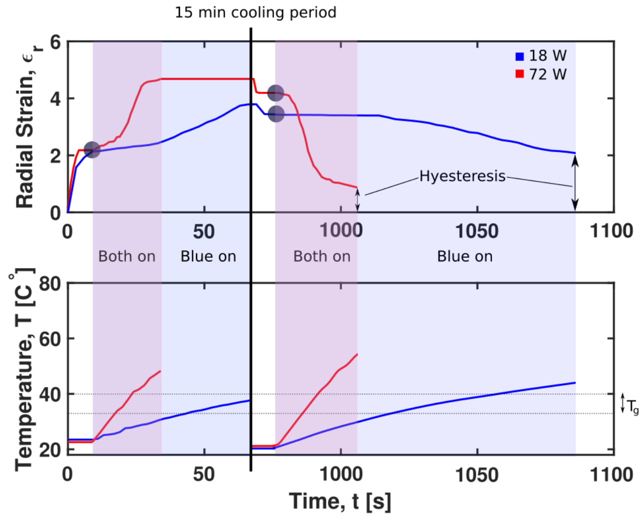

Fig. 6. Transformation operation of the morphing limb from flipper to leg configuration and back. The black dots indicate the start of Joule heating. The two different color trend lines represent different wattages input into the system. Overall, the graph illustrates how greater input wattages enable fast transitions, with the caveat that the limb takes upwards of 15 min to fully cool and stiffen into its new geometry.

2) Radius as a function of time and heat input: We studied the radius of the morphing limb over time to grasp a sense of the time-scale of the morphing operation (Figure 6). First, we applied a fixed pressure (117 kPa) to the flipper phase and we waited until the flipper had expanded to the maximum radius allowable with the stiff material inside it. Then, we activated the heaters and differing input powers of 72 W and 18 W (calculated by multiplying the voltage setting on the power supply by the amperage drawn) and observed how the radius subsequently changed. We recorded the extent of radius change until it had reached a steady state. Then, the inflated limb was allowed to cool for 15 min while the pressure was maintained to fix it into the leg geometry. After it had cooled, we released the pressure and noted the extent of radius change. Then we applied wattage once more and recorded how the leg phase relaxed to the flipper phase.

A thermocouple placed in the center of the morphing limb gave us *in-situ* temperature data. We tracked the radius (the distance between the inner edges of the actuators) using a high-definition camera and ImageJ. We recorded strain as a proportion of initial radius, *i.e.* $\epsilon_r = \frac{\delta R}{R_0}$, with $R_0 = 10$ mm.

Figure 6 shows the radius versus time results for the limb throughout its transformation from flipper to leg, and back (top row). The figure also includes a stacked temperature graph as measured by the thermocouple (bottom row). The blue line indicates behavior associated with a low wattage of 18 W; the red line a high wattage of 72 W. Non-shaded areas indicate where the limb radius expanded/contracted without the presence of input power. The shaded areas represent the times at which power was applied to the system. Black dot marks denote where Joule heating commenced. The T_g transition region is delineated by the fine gray lines stretching horizontally in each of the temperature graphs.

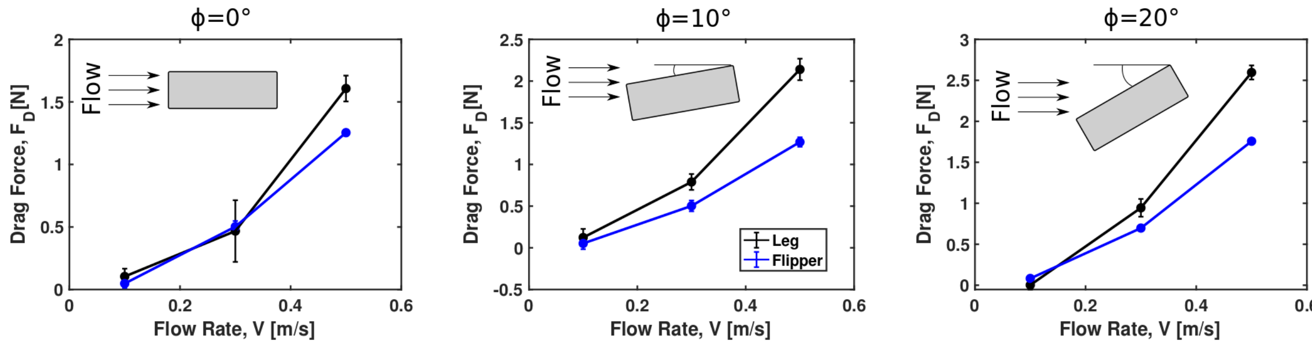

Fig. 7. The morphing limb has potential to enhance locomotion performance for amphibious robots across different environments. For swimming, the limb can assume a flipper shape. It becomes flat, exploiting geometry to reduce drag. The promising drag characteristics of the limb are shown in that it has lower drag forces F_D at higher flow rates V and angles of attack ϕ than the leg. Here, the black marker is the flipper and the blue marker is the leg.

Overall, the instances of radius change after the initial expansion without heat input occur primarily in the T_g region. This effect diminishes in tandem with decreasing heat input. Clearly, the higher power (72 W) allowed the flipper to transition between phases much faster than the lower power (18 W). In the flipper to leg transformation, we also observe that the higher wattage input allowed the limb to reach a larger radius (4.68 strain) compared to the lower wattage (3.79 strain). This finding suggests the lower wattage did not heat the variable stiffness material uniformly enough to fully soften. We suspect free convection and the rate of heat retained by the system reached an equilibrium, causing the radius change expansion to halt.

In the leg to flipper transition, we note that a minimal amount of radius change occurred after releasing the pressure after the 15 min cooling period and before heating. This demonstrates that the cooled variable stiffness material is sufficiently stiff to hold the leg geometry without the aid of the pneumatic actuator. In addition, we note the different amounts of hysteresis depending on the applied wattage. The high wattage case exhibits $\epsilon_r = 1$ of hysteresis, and the low wattage, a much more significant $\epsilon_r = 2.3$. We believe that the ability of the morphing limb to return to its initial flipper state from the leg state depends heavily on its ability to uniformly surpass T_g to induce widespread material relaxation. But, it is clear that some hysteresis remains, which is likely a result of plastic deformation that occurred when straining the thermoset.

Lastly, we suspect that the time required to cool the limb was so long (15 min) because the fabric sleeve and pneumatic actuators act as insulators. Immersion in a liquid medium would likely expedite the cooling process, but might also impact the rate of heating.

3) Flow characteristics assessment: Sea turtles swim using dorsoventral oscillations of wing-like foreflippers for efficient, lift-based locomotion [18]. The geometry of their flipper–flat and thin–helps mitigate drag forces. To determine if our flipper configuration poses better drag characteristics than the leg configuration, we acquired drag force data of the limb in a flow tank. The tank has a 0.87x0.25x0.25 m working section and a speed range over 1.6 m/s. To minimize wall effects, we ensured the flipper was no more than 20 cm in span. Force/Torque data were collected via a 6-axis Gamma DAQ F/T Transducer (ATI industrial). We utilized the measured component of force in the direction of flow for drag, and the component of force normal to the upper surface of the flipper for lift, as in typical hydrofoil experiments. A National Instruments DAQ recorded the data in a LabVIEW interface.

We subjected a morphing limb in each of its two configurations, flipper and leg, to three flow rates at three angles, repeated five times for a total of 90 independent test trials. Flow rates were randomized to mitigate experimental biases and inconsistencies. The flow rates were: 0.1, 0.3, and 0.5 m/s. We believe this is a representative test spectrum for flow rates encountered by a turtle robot, as actual sea turtles have reported sustained swimming speeds of up to 0.278 m/s but bursts up to 0.53 m/s or higher [13], [19]. Note a 0 m/s case was included for calibration purposes for both flipper and leg configurations. We tested the following angles of attack: $\phi = 0°, 10°, 20°$. This spectrum reflects the range of a flipper's angle of attack observed when green sea turtles swim [13]. At the start of each trial, we let the impeller in the tank run for approximately one min to allow the flow to reach steady state. We then collected force/torque data for one min.

Data presented in Figure 7 showcases the results for the flipper and leg phase flow tests. Reported points are average force values for each of the randomized five trials in that angle/flow rate condition. Error bars indicate one standard deviation above and below the mean among the trials.

The results in Figure 7 imply that the flipper phase (blue trend) is beneficial for low-drag swimming, as the flipper generally exhibits less drag force compared to the leg across tested flow rates and angles. However, at 0.1 m/s flow rate for all angles, there is little difference between the two phases. Overall, the drag force on the limb rises at a faster rate as flow rate increases. This finding is consistent with hydrodynamics of streamlined hydrofoils versus other non-streamlined shapes at increasing flow velocities, according to the relation:

$$F_D = \frac{1}{2}\rho v^2 C_D A \quad (6)$$

where ρ is the density of the fluid media, v is the velocity of the fluid flow, C_D is the coefficient of drag, and A is the frontal area. We attribute the better drag force profile of the flipper to its reduced A and C_D terms in comparison to the leg. Since the wetted surface area does not change on the morphing limb, the frontal area A will be reduced as the limb transitions from leg to flipper. Also, streamlined bodies like the flipper have a lower C_D compared to cylindrical bodies like the leg [20].

IV. Conclusion and future work

We presented a morphing limb intended for amphibious robots. The limb is capable of transforming between a flipper and leg configuration. We demonstrated that the flipper mode has a preferable force profile in closed-tank flow tests, suggesting its utility in aquatic locomotion. We also presented evidence that the leg mode could sustain higher compression loads than the flipper mode, suggesting it is better for locomotion on land. A major boon of the morphing limb design presented here is decoupled control of stiffness and geometry. In the flipper stage, a robot equipped with the limb can adjust its stiffness without having to change its shape. This poses advantages for swimming or transitioning from water to land. In the leg phase, stiffness could be controlled further by inflating/deflating the pneumatic actuators, which was not explored in the present work. All of the above capacities are enabled by the novel variable stiffness composite heater system and antagonistic pneumatic actuator pair.

The most prominent shortcoming of the presented work is the long time scale (approximately 15 min) required to cool the material and fully set it into a transformed geometry. We intend to address this heat transfer problem and optimize geometry to facilitate cooling in subsequent work. Other ongoing work includes removing the copper foil heater itself from the system and replacing it with a monolithic, Joule-heating variable stiffness composite. The immediate challenge is balancing the loading of conductive filler with the structural integrity of the limb and thin geometry. Lastly, in the near future, we intend to install this morphing limb on an autonomous, amphibious turtle-inspired robot. We will integrate sensors to discern whether or not the robot is on land, in water, or in a transitional littoral zone, and automatically change the limb morphology and actuation scheme accordingly.

Acknowledgements

The authors would like to recognize Dr. Michelle Yuen for her assistance in fabrication of elastomeric actuators, Dr. Sang Yup Kim for his input regarding the synthesis of epoxy composite materials, Morgan Upchurch for her help with drawing figures, and Dylan Shah for his support modeling the limb. This work was supported by the Office of Naval Research under the Young Investigator Program (N00014-17-1-2604).

References

[1] J. Yu, R. Ding, Q. Yang, M. Tan, W. Wang, and J. Zhang, “On a Bio-inspired Amphibious Robot Capable of Multimodal Motion,” IEEE/ASME Transactions on Mechatronics, vol. 17, no. 5, pp. 847–856, Oct. 2012.

[2] J. Yu, Y. Tang, X. Zhang, and C. Liu, “Design of a wheel-propeller-leg integrated amphibious robot,” in 2010 11th International Conference on Control Automation Robotics Vision, pp. 1815–1819, 2010.

[3] S. Guo, S. Mao, L. Shi, M. Li, and C. Yue, “Development of a spherical amphibious mother robot,” in 2013 ICME International Conference on Complex Medical Engineering, pp. 614–619, 2013.

[4] A. Crespi, A. Badertscher, A. Guignard, and A. J. Ijspeert, “Swimming and Crawling with an Amphibious Snake Robot,” in Proceedings of the 2005 IEEE International Conference on Robotics and Automation, pp. 3024–3028, 2005.

[5] A. Crespi, A. Badertscher, A. Guignard, and A. J. Ijspeert, “An amphibious robot capable of snake and lamprey-like locomotion,” Jan. 2004.

[6] R. Ding, J. Yu, Q. Yang, M. Tan, and J. Zhang, “CPG-based dynamics modeling and simulation for a biomimetic amphibious robot,” in 2009 IEEE International Conference on Robotics and Biomimetics (ROBIO), pp. 1657–1662, 2009.

[7] A. Crespi, K. Karakasiliotis, A. Guignard, and A. J. Ijspeert, “Salamandra Robotica II: An Amphibious Robot to Study Salamander-Like Swimming and Walking Gaits,” IEEE Transactions on Robotics, vol. 29, no. 2, pp. 308–320, Apr. 2013.

[8] A. R. Vogel, K. N. Kaipa, G. M. Krummel, H. A. Bruck, and S. K. Gupta, “Design of a compliance assisted quadrupedal amphibious robot,” in 2014 IEEE International Conference on Robotics and Automation (ICRA), pp. 2378–2383, 2014.

[9] Y. Sun and S. Ma, “ePaddle mechanism: Towards the development of a versatile amphibious locomotion mechanism,” in 2011 IEEE/RSJ International Conference on Intelligent Robots and Systems, pp. 5035–5040, 2011.

[10] X. Liang et al., “The AmphiHex: A novel amphibious robot with transformable leg-flipper composite propulsion mechanism,” in 2012 IEEE/RSJ International Conference on Intelligent Robots and Systems, pp. 3667–3672, 2012.

[11] A. M. Mountcastle and S. A. Combes, “Biomechanical strategies for mitigating collision damage in insect wings: structural design versus embedded elastic materials,” Journal of Experimental Biology, vol. 217, no. 7, pp. 1108–1115, Apr. 2014.

[12] B. Zhong, S. Zhang, M. Xu, Y. Zhou, T. Fang, and W. Li, “On a CPG-Based Hexapod Robot: AmphiHex-II With Variable Stiffness Legs,” IEEE/ASME Transactions on Mechatronics, vol. 23, no. 2, pp. 542–551, Apr. 2018.

[13] J. Davenport, S. A. Munks, and P. J. Oxford, “A comparison of the swimming of marine and freshwater turtles,” Proc. R. Soc. Lond. B, vol. 220, no. 1221, pp. 447–475, Feb. 1984.

[14] F. E. Fish, “Structure and Mechanics of Nonpiscine Control Surfaces,” IEEE Journal of Oceanic Engineering, vol. 29, no. 3, pp. 605–621, Jul. 2004.

[15] P. Polygerinos et al., “Towards a soft pneumatic glove for hand rehabilitation,” in 2013 IEEE/RSJ International Conference on Intelligent Robots and Systems, pp. 1512–1517, 2013.

[16] F. Connolly, P. Polygerinos, C. J. Walsh, K. Bertoldi, Mechanical programming of soft actuators by varying fiber angle. Soft Robot. 2, 26–32. 2015.

[17] T. L. Buckner, E. L. White, M. C. Yuen, R. A. Bilodeau, and R. K. Kramer, “A move-and-hold pneumatic actuator enabled by self-softening variable stiffness materials,” in 2017 IEEE/RSJ International Conference on Intelligent Robots and Systems (IROS), pp. 3728–3733, 2017.

[18] J Wyneken. Sea turtle locomotion: mechnisms, behavior, and energetics. In PL Lutz and JA Musick, editors, The biology of sea turtles, pages 165-198. CRC Press BOca Raton, 1997.

[19] Edward A Standora, James R Spotila, John A Keinath, and C Robert Shoop. Body temperatures, diving cycles, and movement of a subadult leatherback turtle, dermochelys coriacea. Herpetologica, pages 169–176, 1984.

[20] S. Vogel, *Life in Moving Fluids*. Princeton University Press, 1994.